

Reinforced nanowrinkle electrospun photothermal membranes via solvent induced recrystallization

Jinlin Chang¹, Weiling Wang², Zhaoxin Li¹, Yujiao Wang¹, Yacong Hou¹, Zhiyuan Cao², Zhenwei Liang¹, Yuan Ma¹, Ding Weng¹, Jun Song², Yadong Yu¹, Lei Chen¹, and Jiadao Wang¹

¹Tsinghua University

²Shanghai University

March 13, 2024

Abstract

Wearable photothermal materials can capture light energy in nature and convert it into heat energy, which is critical for flexible outdoor sports. However, the conventional flexible photothermal membranes with low specific surface area restrict the maximum photothermal capability, and loose structure of electrospun membrane limits durability of wearable materials. Here, an ultrathin nanostructure candle soot/ multi-walled carbon nanotubes / poly (l-lactic acid) (CS/MWCNTs/PLLA) photothermal membrane is first prepared via solvent-induced recrystallization. The white blood cell membrane-like nanowrinkles with high specific surface area are achieved for the first time and exhibit optimal light absorption. The solvent-induced recrystallization also enables the membrane to realize large strength and durability. Meanwhile, the membranes also show two-sided heterochromatic features and transparency in thick and thin situations, respectively, suggesting outstanding fashionability. Nanowrinkled photothermal membranes by novel solvent-induced recrystallization show high flexibility, fashionability, strength, and photothermal characteristics, which have huge potential for outdoor warmth.

1. Introduction

With the advancement of net-zero carbon emission targets, the effective utilization of renewable resources has attracted widespread attention [1, 2]. Photothermal materials can capture near-infrared light dissipated in the atmosphere and convert it into thermal energy to be utilized, which is highly promising for wearable outdoor devices, disease-assisted therapy, seawater evaporation, catalysis and so on [3-6]. Flexible electrospun-based photothermal membranes (such as Poly (L-lactic acid) (PLLA) and nylon) can offer high comfort, large specific surface area, and wide applicability, so have great potential in the field of wearable photothermal applications [7]; however, durability, excellent photothermal conversion and simplicity of fabrication of flexible photothermal membranes are still key challenges.

The photothermal performance of membranes is directly related to surface micromorphology. Functional micro/nanostructures can exchange or promote the engineering characteristics of materials [8]. Organisms in nature often evolve special microstructures to better adapt to their environment [9]. The wrinkles of the cerebral cortex enhance intelligence [10]; the wrinkles of the guts enhance nutrient absorption [11]; and the wrinkled membranes of leukocytes ensure a higher specific surface area and enhance deformability [12, 13]. Inspired by this, scientists have tried to explore thin membranes with wrinkled microstructures through various methods to enhance the specific surface area and absorption capacity, however, the current imitation of wrinkled sizes still remains at the micrometer scale [9]. The usual methods for obtaining wrinkle microstructures, such as mechanical force [9], photopolymerization [14], infrared induction [15], and post-polymerization [16], have been able to achieve the desired wrinkle morphology. 3D printing allows for the

generation of controllable nanowrinkles [17], but its high preparation cost limits the preparation of large-area nanowrinkles. Mechanical force and photopolymerization, etc. enable fast batch preparation, but it is difficult to form nanoscale wrinkles. Post-polymerization enables low-cost preparation of nanowrinkles, but the long cross-linking reaction time and instability limit the enhancement. The realization of low-cost, large-area and durable nanowrinkle membranes remains a challenge. Also, ultra-thin electrospun membranes are often easily damaged [18]. Therefore, an effective treatment procedure based on electrospun membranes is urgently needed to develop the durability of the material while realizing high specific surface area photothermal films.

Here, a solvent-induced recrystallization approach is developed firstly to obtain high-strength CS/MWCNTs/PLLA photothermal membranes with nanowrinkled structures. The adhesive polydimethylsiloxane (PDMS) dissolved in the solvent will residue on the fiber membrane after the solvent evaporates, which not only tightly connects the photo-thermal particles, but also forms an adhesive network to facilitate the intensive cross-linking between the fibrils, so significantly enhancing the membrane strength. The membranes also show two-sided heterochromatic features or transparency because of the gradient photothermal particle concentration, which considerably extends the fashionability and customizability. Remarkably, the membrane also has excellent response sensitivity and can heat up immediately after exposure to light. The ultrathin nanowrinkled photothermal membrane by solvent-induced recrystallization enables rapid batch preparation of enhanced functional composite membranes, showing broad prospects in snow clothing, Winter Olympics garments, and so on.

2. Methods

2.1. Materials

Poly (L-lactic acid) (PLLA, PL 65) was obtained from PURAC Biomaterials. Tetrahydrofuran (99.5%) was bought from Beijing Bailingwei Science and Technology CO. LTD. Acetone (99.5%) was supplied by Modern Oriental (Beijing) Technology Development CO. LTD. SylgardTM184 silicone elastomer kit (PDMS) was purchased from Dow. MWCNTs were acquired from Shenzhen Suiheng Science and Technology CO. LTD. Dimethyl formamide (DMF, 99.80%) was bought from Fisher Scientific Ltd. Dichloromethane (DCM, 99.99%) was purchased from Sigma-Aldrich. Human Skin Fibroblasts (HSF) cells and HSF specialized culture medium were obtained from Shanghai Saibekang Biotechnology. Phosphate buffer saline (PBS) was bought from Procell. Pancreatic enzyme was supplied by Biosharp. Cell Counting Kit-8 (CCK8) were purchased from Invigentech. All chemicals were of analytical grade without any further purification.

2.2. Preparation of PLLA nanofibers and CS

The PLLA was dissolved in DCM and DMF with a mass ratio of 1.8: 93.29: 4.91, then was electrospun by electrospun equipment. Electrospun equipment kept fixed parameters: 30 ml syringe; 19 G needle; 30 cm distance between the needle and the collector; 17 kV voltage; 5 ml/h feeding speed; 2 h collection [18].

CS was obtained by the following method. First, a candle was lit and a glass plate was placed above the candle flame. Then, the black CS gradually adhered to the glass plate and lasted for 3 minutes. Finally, the glass plate was removed and cooled, and the CS was gained by scraping off the coating on the glass plate.

2.3. Preparation of photothermal membranes by solvent-induced recrystallization

The first step is the recrystallization of PDMS and photothermal particles dispersion. CS and MWCNTs were mixed at a mass ratio of 1:1, dispersed in tetrahydrofuran and stirred, followed by the addition of PDMS and ultrasonication. The content ratio of substances was CS: MWCNTs: PDMS: tetrahydrofuran=0.1g: 0.1g: 3g: 100ml, and the mass ratio of PDMS to curing agent was 3:1. The PLLA fiber membrane was fixed on a metal frame, immersed into the above mixing solution with continuous ultrasonication for 20 seconds.

The second step is the recrystallization of PLLA. The membrane treated by tetrahydrofuran are quickly taken out and immersed into acetone for 5 minutes, and finally removed and dried at room temperature to obtain the double-sided heterochromatic photothermal membrane. The volume of tetrahydrofuran was

changed to 200 ml and 400 ml and the experiment was repeated. For easy differentiation, in the Results and Discussion section, we named the PDMS-containing solvent-treated PLLA as APLLA.

Other solvent-induced recrystallization were also explored. Method 1: Acetone treatment, drying and then treated with tetrahydrofuran containing PDMS and CS/MWCNTs. Method 2: Treated by the solvent of tetrahydrofuran containing PDMS and CS/MWCNTs. Method 3: Treatment with tetrahydrofuran containing PDMS and CS/MWCNTs, drying and then acetone treatment. Method 4: Acetone treatment and then treatment with tetrahydrofuran containing PDMS and CS/MWCNTs. Method 5: Treated by the solvent of acetone containing PDMS and CS/MWCNTs (Little amounts of tetrahydrofuran were used to dissolve PDMS in acetone).

2.4. Characterizations

The morphologies of the photothermal films were acquired with a Scanning Electron Microscope (SEM, SU8200, HITACHI, Japan), and the elemental maps and percentage were obtained by the corresponding Energy Dispersive Spectrophotometer (EDS). The Transmission Electron Microscopy (TEM) of samples is gained by JEM2010. X-ray diffraction patterns (XRD) of the samples were characterized by D8 Advance, Bruker. Strain-Stress curves were collected by Electronic Universal Material Testing Machine (WDW-3020). Autosorb iQ₂ was used to achieve Brunauer-Emmett-Teller (BET). The water contact angle of the solar heating membranes was measured by Dataphysics OCA25, Germany. The Ultraviolet-Visible- near infrared (UV-vis-NIR) absorption spectroscopy was achieved by Perkin Elmer, Lambda 1050+. The Discovery TGA was utilized for thermogravimetric analysis (TGA). The differential scanning calorimetry (DSC) was collected by DSC Q2000.

The photothermal data of the materials were acquired by FLIR T620 and analyzed using the matching software FLIR Tools. Sunlight in the laboratory is obtained through a simulated daylight xenon light source. Solar irradiation was obtained by a TES 132 Datalogging solar power meter. Temperature information was gained from windy.com. Location coordinates were obtained from Google map.

CCK-8 was used to detect the changes of cell viability in the co-culture of HSF cells and samples for 12h and 24h. HSF cells in logarithmic growth stage were taken, inoculated into the 24-well plate according to 4×10⁴/well, and the culture medium was incubated at 5% CO₂ and 37 for 12h and 24h. After that, the medium was removed, and each well was washed with PBS for three times, and incubated for 2 hours at 37 in a constant temperature incubator by adding medium containing 10% CCK-8, 5% CO₂ at 1mL/well. The absorbance at 450nm was detected by zymography and the relative viability was calculated.

3. Results and discussion

3.1. Nano-wrinkled photothermal membranes by solvent induced recrystallization

The electrospun fibrous membranes with solvent-induced recrystallization have microscopic wrinkles (Fig. 1a and b). The wrinkle morphology is similar to that of human white blood cells (Fig. 1c), and this surface wrinkled structure greatly enhances the specific surface area and thus the light absorption ability of the film. Unlike white cell membranes, the size of the wrinkles in our photothermal membranes is much smaller and reaches the nanometer scale. Nano-wrinkles have superior surface properties but are more difficult to achieve, which highlights the advantages of solvent-induced recrystallization for the preparation of nano-wrinkles. The process of solvent-induced recrystallization is as follows: The ultrathin photothermal membrane firstly is prepared by the electrospinning technique, afterwards, the photothermal particles CS/MWCNTs and the adhesive PDMS are sufficiently dispersed in the porous membrane by a short ultrasonication (20 s), and then the optimized photothermal membrane is obtained by acetone treatment for 5 min. Later, after the evaporation of the organic solvent, the photothermal membranes are gained, as shown in Fig. 1d.

The whole solvent-induced recrystallization process can be divided into two steps, the first step is the recrystallization of PDMS with the solubility of PDMS in tetrahydrofuran, which aims to enhance the strength of the fiber membrane and make the photo-thermal particles tightly attached; the second part is the recrystallization of PLLA with the fact that PLLA is slightly soluble in acetone, which forms a

hierarchical morphology on the surface of the fibers after volatilization. fiber membrane before solvent-induced recrystallization is shown in Fig. e-g and Fig. S1, and there is no wrinkle structure. After solvent treatment, the photothermal particles form a wrapping relationship with PLLA fibers and acquire the photothermal capability (Fig. 1h). The photothermal performance and the schematic diagram of the principle are shown in Fig. 1i, j and Fig. S2.

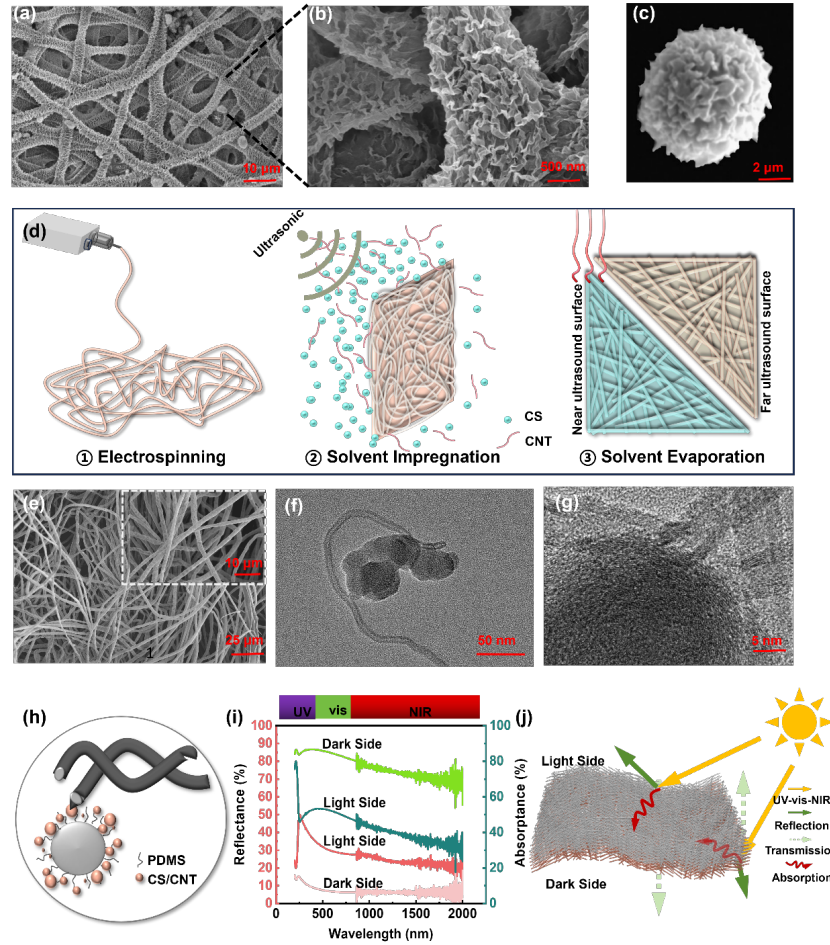


Figure 1. The nano-wrinkled structure enhanced flexible photothermal membranes by solvent induced recrystallization. (a, b) The micromorphology of nano wrinkled photothermal membranes. (c) White blood cell with wrinkled membrane morphology [12]. (d) The solvent induced recrystallization process. (e) The original PLLA membrane. (f, g) The TEM of CS and MWCNTs. (h) The structure of photothermal fibrils. (i) The comparison of reflectance and absorptance by UV-vis-NIR spectroscopy for photothermal membranes. UV: wavelength < 400 nm; vis: 400 nm \leq wavelength \leq 780 nm; NIR: wavelength > 780 nm. (j) The schematic diagram of photothermal conversion of membranes.

3.2. The physical properties of photothermal membranes

The light absorption characteristics of the photothermal membranes can be obtained by UV-vis-NIR spectroscopy (Fig. 2a-c). APLLA, CS/MWCNTs/APLLA light-colored surfaces and dark-colored surfaces all exhibit lower reflection and higher absorption at shorter wavelengths of UV. However, as the UV wavelength increases, the reflections of APLLA and light-colored surfaces increase steeply, while the dark surface remains constant or even decreases slowly. In the near-UV band, dark-colored surface shows excellent absorption

(86.71%), while the light-colored surface is slightly inferior to that of the dark-colored surface, but still presents a high absorption (80.07%). In the vis-NIR band, the absorption of both light and dark surfaces decreases slowly, but the absorption of the dark surface is always larger than that of the light surface, and the absorption of APLLA rises slowly and is much smaller than that of CS/MWCNTs/APLLA. In the vis-NIR band, the reflections of the dark surfaces are always maintained at very low values. The light side and APLLA decrease, and the reflection of the light side is much lower than that of APLLA. In conclusion, the dark side of CS/MWCNTs/APLLA shows excellent absorption in the full band, and the light side is a little inferior to the dark side, but the absorption is excellent and much higher than that of APLLA, which demonstrates the excellent photothermal performance. The reflectance, transmittance and absorptance satisfy the following equation [19]:

$$R + T + A = 1 \quad (1)$$

The XRD patterns of the dark surface show more peaks than those of the APLLA and light surfaces, appearing at 2 Theta of 108 and 118 (Fig. 2d). This is because the dark surface has a higher concentration of CS and MWCNTs. This also indicates that the light surfaces have a very low content of CS and MWCNTs, which is almost close to pure APLLA. The CS/MWCNTs/APLLA TGA curve is almost identical compared to APLLA, and the presence of CS and MWCNTs causes the material to decompose more rapidly during thermal degradation (Fig. 2e). The DSC data (Fig. 2f) exhibits the variation of the heat flow with temperature versus the sapphire (see Fig. S3 for those with baseline). The specific heats of APLLA and CS/MWCNTs/APLLA can be obtained by Temperature - [?]Heat Flow curves and comparative calculation (Fig. 2g). c_p is the specific heat, m is mass, and p is heat flow. The specific heat of sapphire has a standard, so the specific heat of APLLA and CS/MWCNTs/APLLA can be calculated, as shown in Table S1. The loose structure of the electrospun membrane also leads to weak connections between fibrils and poor strength [20]. The strain-stress curves (Fig. 2h and Supplementary Note S1) show that the strength of the treated photothermal film increases dramatically compared to the pristine PLLA, with Young's modulus exceeding four times that of PLLA. The water contact angle of APLLA was 127.65°, showing high hydrophobicity, and the contact angle slightly increased to about 137°. The contact angles are almost the same for the darker and lighter surfaces after adding photo-thermal particles (Fig. S4). The material exhibits superior hydrophobicity, which enhances the application of wearable membranes in variable weather [21, 22]. These physical characteristics further demonstrate that the double-sided heterochromatic photothermal film has a gradient concentration distribution, which explains the formation of a double-sided heterochromatic structure and shows the absorption features of UV-vis-NIR spectra.

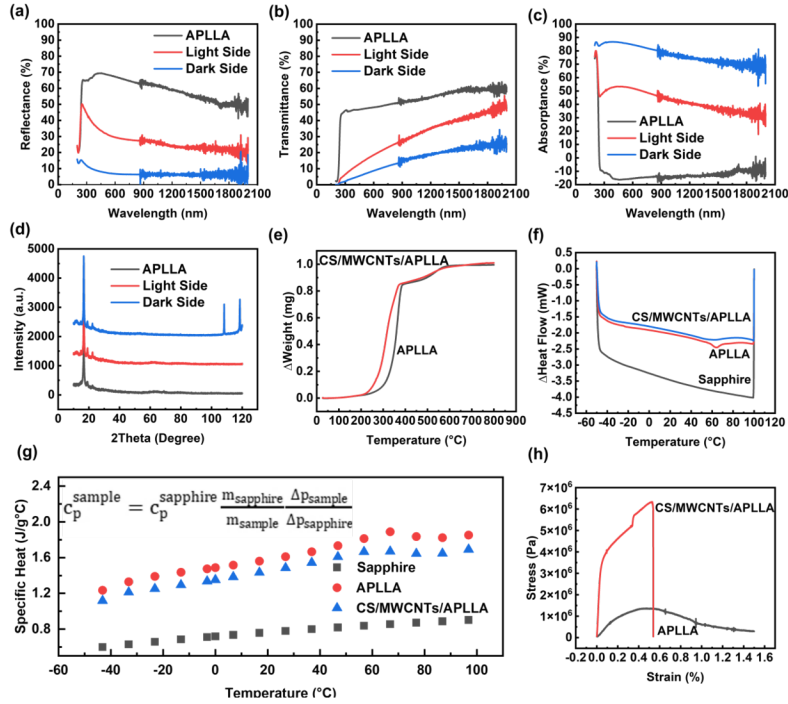


Figure 2. The physical properties of nano wrinkled photothermal membranes. (a) The reflectance of UV-vis-NIR spectroscopy for photothermal membranes. (b) The transmittance of UV-vis-NIR spectroscopy for photothermal membranes. (c) The absorbance of UV-vis-NIR spectroscopy for photothermal membranes. (d) The XRD of photothermal membranes. (e) The TGA of the samples. (f) The DSC of photothermal membranes. (g) The specific heat of photothermal membranes. (h) The strain-stress curves of photothermal membranes.

3.3. Analysis of the effect of nanowrinkled structures on photothermal performance

A novel solvent-induced recrystallization procedure is proposed for the first time in this study, which enables the high specific surface area and functional modification of electrospun membranes in a very short period of time (less than 6 min). It simplifies the previously cumbersome four-step process: morphology modification, mechanical reinforcement, adhesive generation and adherence and allows obtaining high-performance photothermal membranes. Moreover, this method can help photothermal membranes realize special nano-wrinkled structure. As shown in Fig. 3a, compared with the porous structure, the nano wrinkled membrane will provide more attachment sites for the photothermal particles, which is beneficial to the photothermal performance.

In this study, acetone exist as a modifier for hierachical porous morphology, and PDMS can achieve good dispersion and rapid volatilization only by tetrahydrofuran [23, 24]. Thus, we studied various combinations of the two solvents. Tetrahydrofuran does not have a solubilizing effect on PLLA, so only tetrahydrofuran as a solvent cannot modify the fiber morphology and causes dense accumulation between the fiber layers, resulting in a significant agglomeration of photothermal particles on the surface (Method 2, Fig. 3b and S5a). Since PDMS is insoluble in acetone, when treated only with acetone, PDMS adheres to PLLA before the solvent evaporates, resulting in the inability to form wrinkled structures (Method 5, Fig. 3c and S5b). For acetone treatment, drying and then treating with tetrahydrofuran containing CS/ MWCNTs, PLLA was insoluble in tetrahydrofuran, making it difficult to form a distinct wrinkled structure (Method 1, Fig. 3d and S6a). For treatment with tetrahydrofuran containing CS/MWCNTs, drying and then acetone treatment, PDMS was deposited before acetone evaporation and could not form wrinkles (Method 3, Fig. 3e and

S6b). For acetone treatment and then treatment with tetrahydrofuran containing CS/MWCNTs, PLLA was insoluble in tetrahydrofuran and it was difficult to form a distinct wrinkled structure (Method 4, Fig. 3f and S6c). The tetrahydrofuran treatment and subsequent treatment with acetone harvested more desirable morphology and photothermal characteristics, as shown in Fig. 3e and S7 (Method in this study). We also evaluate the photothermal performance of the membranes under different morphology and specific surface area. Heat distribution plots of the membranes before (Fig. S8) and after (insert images in Fig. 3b-g) 5 min of 1 sunlight irradiation and the maximum temperature are plotted in Fig. 3h. Methods 1, 2, and 4 have poor photothermal performance, while methods 3 and 5 both have superior photothermal properties, but their vanishing or very small wrinkled structures limit the potential upper limit of the photothermal film and need to be further optimized. The method in this study shows best photothermal performance. BET data show that the film containing the photothermal particles has only a slight decrease in specific surface area compared to APLLA, they all exhibit an exceptionally high specific surface area (Fig. 3i and Table S2). The nano-wrinkled surface greatly increased the specific surface area about 164 times, from 0.3057 m²/g (macroscopic) to 50.00 m²/g (macroscopic).

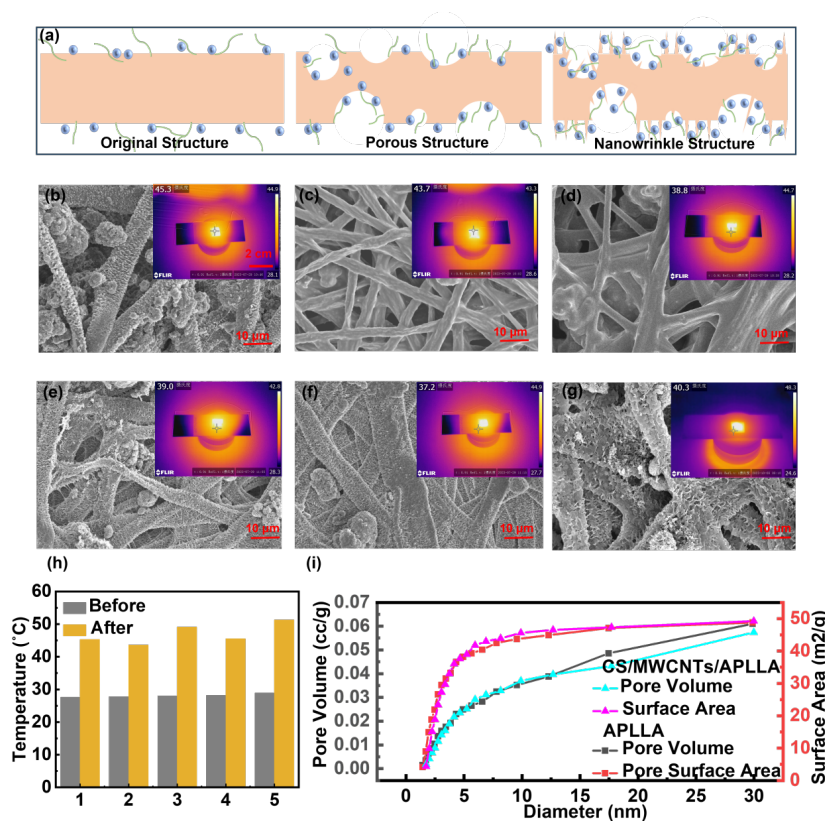


Figure 3. Analysis of the influence of nano wrinkled structure on the photothermal performance. (a) Comparison of original structure, porous structure and nano-wrinkled structure. (b-g) Comparison of micromorphology of nano-wrinkled and non-nanowrinkled structures (The inset images are comparison of photothermal performance of nano-wrinkled and non-nanowrinkled structures after 5min 1 sunlight irradiation.). (b) The photothermal membrane treated by solvent of tetrahydrofuran. (c) The photothermal membrane treated by solvent of acetone. (d) Acetone treatment, drying and then treated with tetrahydrofuran containing CS/MWCNTs. (e) Treatment with tetrahydrofuran containing CS/MWCNTs, drying and then acetone treatment. (f) Acetone treatment and then treatment with tetrahydrofuran containing CS/MWCNTs. (g) Nano-wrinkled structure in this study. (h) The photothermal comparison of membranes before and after

5min sunlight irradiation by the 5 solvent-induced recrystallization in b-g. (i) The BET of photothermal membranes.

3.4. Double-sided heterochromatic characteristics and light transmittance of photothermal membranes

Membranes of different thicknesses will achieve two-sided heterochromatic features and translucency through solvent-induced recrystallization. The loose and porous structure of the electrospun membrane provides a deep penetration network for the photothermal particles, creating a microscopic 3D photothermal absorption space (Fig. 4a and b). The gradient photothermal network creates a two-sided heterochromatic appearance (Fig. 4c, thick membranes ($\sim 20 \mu\text{m}$, Fig. 4d and Fig. S9)) and allows for excellent photothermal performance on the light side, which greatly improves the fashionability of photothermal materials [25]. Then, with the rapid evaporation of the solvent and the action of PDMS, the fiber film rapidly densifies and tightly crosslinks, binding the photothermal particles inside the membrane, which greatly enhances the internal photothermal factor embedding and the integrated photothermal performance. Also, it creates a gradient distribution between dark and light faces (Fig. 4e).

When the fiber membrane is very thin, the photothermal particles can easily pass through the membrane, so the two-sided heterochromatic feature disappears and is replaced by transparency (Fig. 4f and Fig. S10, thin thickness ($\sim 6.5 \mu\text{m}$, Fig. 4g, h and Fig. S11 and S12)). The EDS distribution of the transparent cross section is shown in Fig. S13 and S14. The main substance compositions of the photothermal particles CS and MWCNTs are shown in Fig. S15 and S16. Both the double-sided heterochromatic feature and the transparency can improve the shortcoming of the conventional photothermal membrane, which can only be dark in color, and enhance the fashionability of wearable textiles. For the SEM images of APLLA and photothermal membranes (Fig. S17), the EDS distribution (Fig. 4i-k and Fig. S18) show that the adhesive PDMS is uniformly distributed throughout the membrane, providing sufficient adhesive sites. The CS/MWCNTs/APLLA light and dark surfaces show the obvious existence of elemental C, indicating the large distribution of CS particles and MWCNTs particles. Obviously, agglomerated C is also observed in its holes, suggesting that the photothermal particles can penetrate into the interior of the film. The elemental spectrum of the light-colored photothermal film surface is shown in Fig. S19. C and O are the main components, and Si also has big components, displaying the arrangement of the adhesive and the photothermal components.

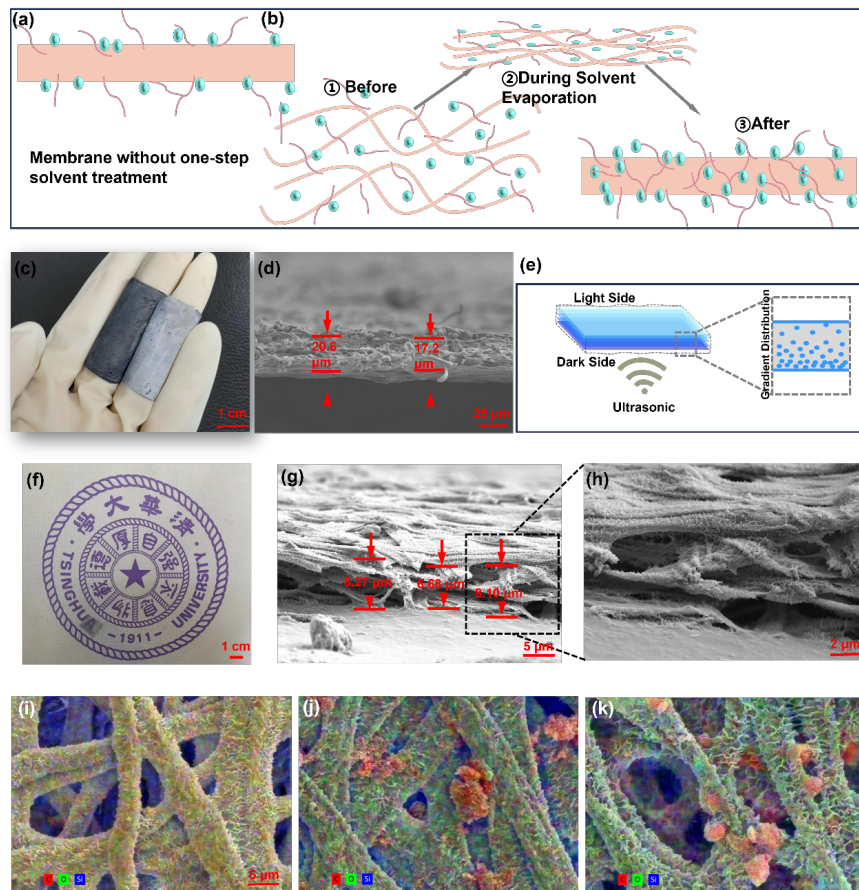


Figure 4. Double-sided heterochromatic characteristics and light transmittance of photothermal membranes. (a) The membrane without solvent induced recrystallization (photothermal particles can only be attached to the surface). (b) The membrane with solvent induced recrystallization (photothermal particles form networks inside the membrane). (c) The pictures of double-sided heterochromatic photothermal membranes (20 μm). (d) The cross-section of double side heterochromatic photothermal membranes. (e) The gradient distribution of photothermal particles during solvent induced recrystallization. (f) Transparency of the membrane (on the fabric, the membrane covers the letter ‘A’ in ‘TSINGHUA’). (g) Cross-section of transparent membranes. (h) Amplification of (g). (i) The EDS maps of the treated membrane without CS and MWCNTs. (j) The EDS maps of the light side of photothermal membranes. (k) The EDS maps of the dark side of photothermal membranes. The red represents C, the blue represents Si, and the green represents O.

3.5. Solar heating performance and outdoor tests

The photothermal properties of transparent or double-sided heterochromatic nano wrinkled fiber films were evaluated by thermal imaging. PLLA and APLLA without CS/MWCNTs showed almost no temperature rise (Fig. 5a-d). As shown Fig. 5e, at the initial CS/MWCNTs concentration, the temperature of the dark side of the film continued to increase with the increase of the sunlight radiation time, and the higher the concentration, the higher the temperature. However, when the concentration of CS/MWCNTs was reduced to 1/4 of the original concentration, the photothermal response of the film was elevated, and it could be almost instantaneously boosted to high temperatures, but with large temperature fluctuations. Comparing the dark and light sides of CS/MWCNTs/APLLA (Fig. 5f), it can be found that the light side has a more rapid photothermal response and no significant enhancement with time, but is unstable; the dark side has a slow increase in temperature with time and better photothermal stability. Comparing the photothermal

performance of CS/MWCNTs/APLLA dark-colored surface under different sunlight radiations (Fig. 5g), it can be found that the temperature of the photothermal film is higher with the same time as the radiation enhancement, and the higher the radiation intensity, the more rapid the response. However, the temperature distinction is not obvious for sunlight densities of 1000 kWm^{-2} and 1250 kWm^{-2} .

We also evaluate the photothermal performance of the membranes on low-temperature substrates, as shown in Fig. 4h. CS/MWCNTs/APLLA light side (top left), dark side (top right), dark side 1/2 concentration (bottom left), and dark side 1/4 concentration (bottom right) were placed on cryogenic glass (-20 @C), and the temperature changes were recorded under 1 sunlight radiation (1000 kWm^{-2}). The Max represents the maximum temperature of the 4 photothermal films, and Sp1 represents the collimation temperature. It can be seen that the photothermal membrane on the cryogenic substrate can also heat up rapidly and the maximum temperature reaches nearly 55 @C within 4 minutes, with the darker side of the membrane with a high concentration of CS/MWCNTs/APLLA showing the best low-temperature photothermal effect. We also evaluate the photothermal uniformity of the films. As shown in the Fig. 4i-k, comparing the thermal distribution of the material before and after 5 minutes of 1 sunlight irradiation, it can be seen that the thermal distribution of CS/MWCNTs/APLLA photothermal film is very homogeneous and shows high in the middle and low at both ends [26].

The evaluation of wetting the photothermal film is also important since wearable materials are often faced with situations such as sweat-soaking [27]. As shown in Fig. S20 and Supplementary Video 1, the heat distribution of the photothermal film before and after the drop of pure water is recorded. Even under wetting conditions, the film can rise to 37 @C within 4 minutes and promote liquid evaporation for self-drying recovery. Fig. S21 demonstrates the variation of the maximum temperature (Max) of the area and the collimation temperature (Sp1) under the wetting condition, and the photothermal film exhibits a fast temperature recovery. The thermal management capability of the film is also an important criterion. The membrane was heated in an oven at 60 @C for 5h, after which it was taken out and the photothermal distribution was recorded as shown in the Fig. S22 and 23. The photothermal film has excellent thermal dispersion and can be cooled from 60 @C to room temperature in 10 s. The distribution of the temperature along the collinear horizontal line indicate that the film has excellent uniformity [28]. Furthermore, we test the thermal performance of the film in different orientations (parallel, 40 degrees and perpendicular to the light). The orientation perpendicular to the light gives the best performance (Fig. S24a-c). The film also shows good thermal behavior when folded (Fig. S24d).

We conduct outdoor evaluations of CS/MWCNTs/APLLA membranes. The outdoor test equipment was shown in Fig. S25 and the detailed outdoor test parameters were shown in Table S3 and the test locations are shown in Fig. 6a. At night without sunlight irradiation, the temperature of the photo-thermal film decreases with the air temperature and is slightly higher than the air temperature by 2 @C (Fig. 6b). At 7-8 am, the photothermal membrane can reach nearly 50 @C with less than 0.5 sunlight irradiation. The sharp fluctuation of the membrane temperature in two places between 7:0-7:10 am is caused by obstacles blocking the membrane, while the slow decrease and increase of the temperature between 7:10-7:20 am is caused by the decrease of sunlight radiation due to the blocking of sunlight by buildings (Fig. 6c). At midday, when the sunlight was 800 kWm^{-2} , the temperature of the solar thermal film was even close to 75 @C and remained consistently high. One of the short temperature drops was affected by clouds covering the sun (Fig. 6d). At sundown, both air temperature and solar irradiation gradually decrease, the temperature of the film first rises and then falls, and the temperature of the film can only be maintained in the range of $38\text{-}40 \text{ @C}$ when the solar irradiation falls to 100 kWm^{-2} and below (Fig. 6e). As the weather changes from sunny to cloudy, solar radiation drops dramatically and the effectiveness of the solar thermal membranes decreases. In rainy weather, the surface of the membrane gets wet with rainwater, thus affecting the photothermal performance (Fig. 5f-h). By comparing the photothermal performance of the membrane under different weather conditions, it shows the universality of the double-sided heterochromatic photothermal membrane under varies environments [29].

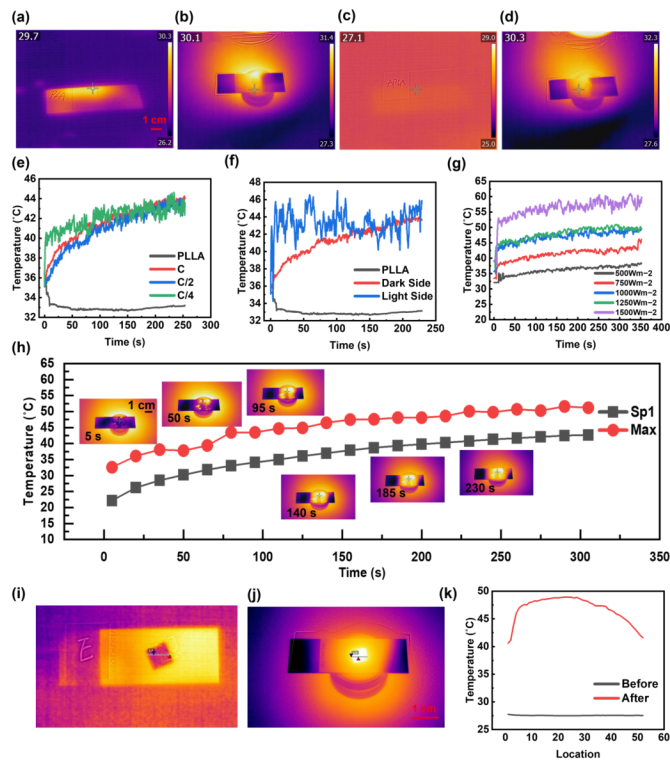


Figure 5. The photothermal performance of double-sided heterochromatic nano wrinkled photothermal membranes. (a) The original PLLA membranes before sunlight irradiation. (b) The original PLLA membranes after sunlight irradiation. (c) The treated PLLA membranes without CS and MWCNTs before sunlight irradiation. (d) The treated PLLA membranes without CS and MWCNTs after sunlight irradiation. (e) The photothermal comparisons of membranes in different CS/MWCNTs concentrations. (f) The photothermal comparisons of dark side and light side. (g) The photothermal comparisons of membranes in different sunlight irradiation. (h) The photothermal performance of membranes on low-temperature glass substrates (-20 °C) (Top left, original concentration light side; top right, original concentration dark side; bottom left, C/2 concentration dark side; bottom right, C/4 concentration dark side). (i, j) The photothermal comparisons of membranes before (i) and after (j) sunlight irradiation, the blue triangle represents the location of the lowest temperature on the line, the red triangle represents the location of the highest temperature on the line. (k) The temperature distribution on the line of (i and j).

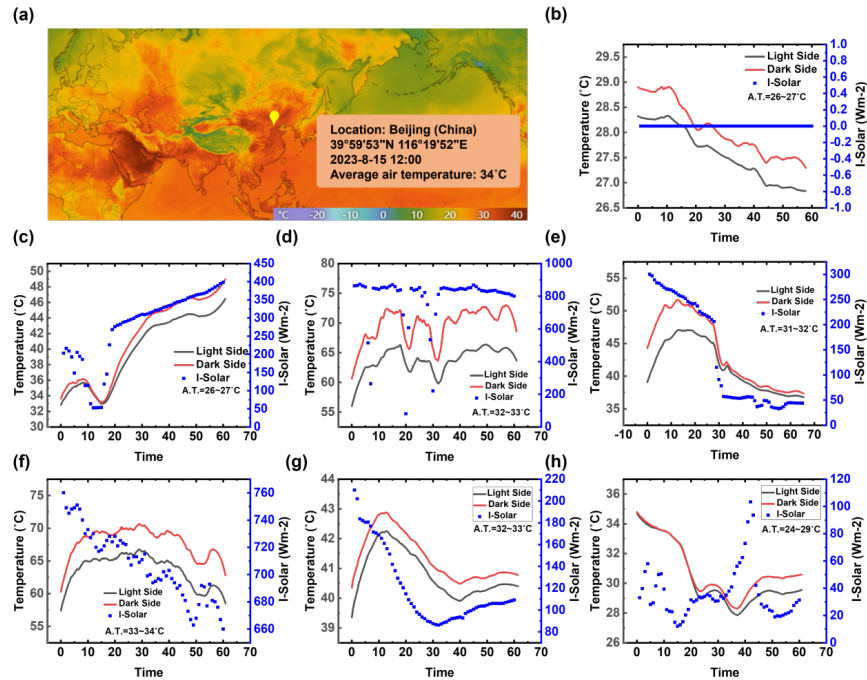


Figure 6. The outdoor solar heating performance of double-sided heterochromatic nano wrinkled photothermal membranes. (a) The test location. (b-e) The outdoor solar heating test on a sunny day at 0-1am (b), 7-8am (c), 12-13pm (d) and 17-18pm (e). (f-h) The outdoor solar heating test at 14-15pm on a sunny day (f), a cloudy day (g) and a rainy day (h).

3.6. Wearability

The performance of the photothermal membranes is evaluated on human skin as shown in Fig. 7a, b, and Supplementary Video 2. The top is the initial CS/MWCNTs concentration, the bottom left is 1/2 of the initial concentration, the bottom right is 1/4 of the initial concentration, and in the middle of the three is PLLA (which is difficult to distinguish from the figure due to its very poor photothermal performance). It can be seen that the high concentration of CS/MWCNTs/APLLA always maintains the highest temperature, which slowly increases with time up to 46 @C without discomfort to human skin. The photothermal membrane was pasted on clothes and evaluated for its photothermal performance (Fig. 7c and d). It can rise 7.6 @C in two minutes outdoors (865 Wm^{-2}), which is significantly better than PLLA, demonstrating its applicability to wearable photothermal devices. By co-culturing with HSF for 12 and 24 hours, the photothermal membrane also demonstrated excellent biocompatibility (Fig. 7e and f).

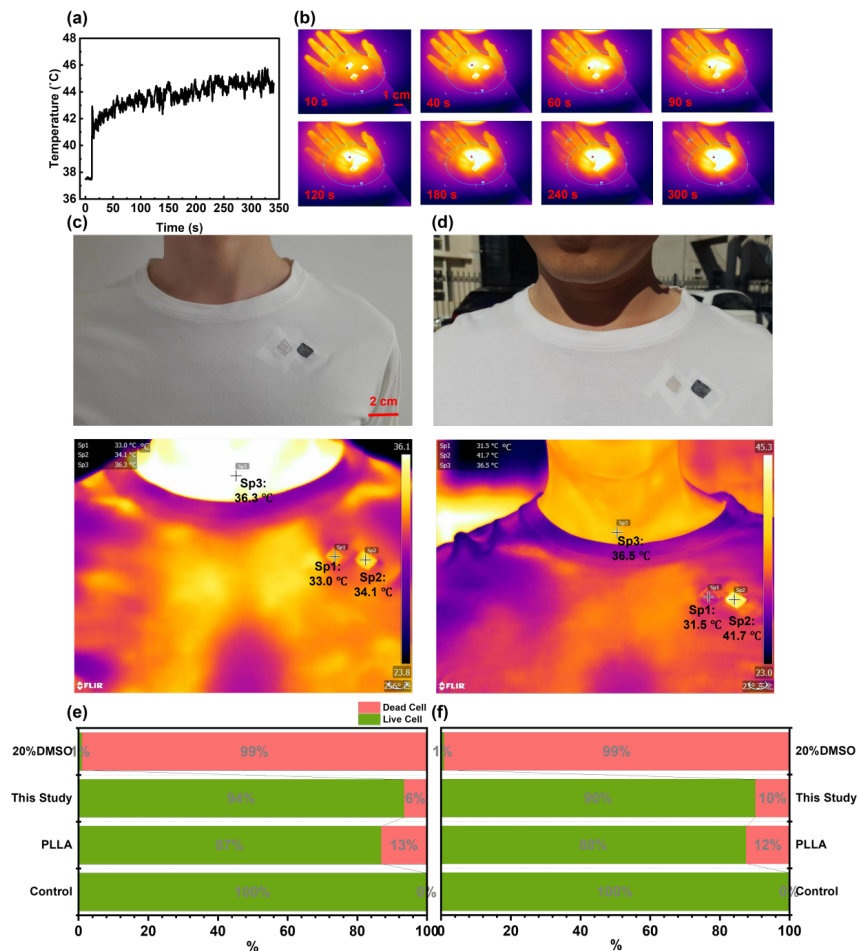


Figure 7. The wearability of photothermal membranes. (a) The photothermal performance of membranes on human skin. (b) The photothermal maps of membranes on human skin. (c) Indoor performance of wearable photothermal membranes (0.3Wm^{-2} sunlight, 21 @C). (Sp1 is the temperature of PLLA; Sp2 is the temperature of the photothermal membrane; Sp3 is the temperature of human skin; The membranes ($20\ \mu\text{m}$) are glued to cotton fabrics and contact directly with the human skin.) (d) Outdoor performance of wearable photothermal membranes (865Wm^{-2} , 21 @C). (e) Investigation of cell viability (e: 12h; f: 24h), showing the good biocompatibility of photothermal membranes.

4. Conclusion

In summary, reinforced CS@MWCNTs/PLLA photothermal membranes obtained by solvent-induced recrystallization are reported in this work. The photothermal membrane exhibits a nanowrinkled structure with a high specific surface area, which provides more light absorption and enhances the photothermal effectiveness of the membrane. The photothermal film can heat up instantaneously and maintain between $60\sim 75\text{ @C}$ at 800Wm^{-2} sun irradiation, which provides excellent photothermal performance. The innovative solvent-induced recrystallization procedure can greatly improve the mechanical properties and micro-morphology of the electrospun membrane without sacrificing the wearing comfort of the flexible membrane and is potentially applicable to other electrospun membranes.

Author contributions

This manuscript was written with the contributions of all authors. All authors have approved the final

version of the manuscript. **Jinlin Chang**: Methodology, Conceptualization, Investigation, Formal analysis, Data curation, Writing – review & editing. **Weiling Wang** : Conceptualization, Data curation. **Zhaoxin Li, Yujiao Wang, Yacong Hou, Zhiyuan Cao, Zhenwei Liang** : Data curation. **Ding Weng, Yuan Ma** : Methodology. **Yadong Yu, Jun Song** : Methodology, Conceptualization, Investigation. **Lei Chen, Jiadao Wang** : Project administration, Supervision, Methodology, Conceptualization, Formal analysis, Investigation, Writing – review & editing.

: **Jinlin Chang** and **Yadong Yu** contributed equally to this work.

Acknowledgments

We acknowledge Dr. Jiashen Li at The University of Manchester and Zixuan Li at Imperial College London, UK. This work is financially supported by Shanghai Pu jiang Program (22PJD026).

References

- [1] S. García-Freites, C. Gough, M. Röder, The greenhouse gas removal potential of bioenergy with carbon capture and storage (BECCS) to support the UK’s net-zero emission target, *Biomass and Bioenergy* 151 (2021) 106164.
- [2] M. Shahbaz, M.A. Nasir, E. Hille, M.K. Mahalik, UK’s net-zero carbon emissions target: Investigating the potential role of economic growth, financial development, and R&D expenditures based on historical data (1870–2017), *Technological Forecasting and Social Change* 161 (2020) 120255.
- [3] C. Murugan, V. Sharma, R.K. Murugan, G. Malaimengu, A. Sundaramurthy, Two-dimensional cancer theranostic nanomaterials: Synthesis, surface functionalization and applications in photothermal therapy, *Journal of Controlled Release* 299 (2019) 1-20.
- [4] C. Chen, Y. Li, J. Song, Z. Yang, Y. Kuang, E. Hitz, C. Jia, A. Gong, F. Jiang, J. Zhu, Highly flexible and efficient solar steam generation device, *Advanced materials* 29(30) (2017) 1701756.
- [5] L. Zhu, M. Gao, C.K.N. Peh, G.W. Ho, Recent progress in solar-driven interfacial water evaporation: Advanced designs and applications, *Nano Energy* 57 (2019) 507-518.
- [6] W. Chen, H. Miao, G. Meng, K. Huang, L. Kong, Z. Lin, X. Wang, X. Li, J. Li, X.Y. Liu, Polydopamine-induced multilevel engineering of regenerated silk fibroin fiber for photothermal conversion, *Small* 18(11) (2022) 2107196.
- [7] T.M. Makinen, J. Hassi, Health problems in cold work, *Industrial health* 47(3) (2009) 207-220.
- [8] W. Wang, J. Chang, L. Chen, D. Weng, Y. Yu, Y. Hou, G. Yu, J. Wang, X. Wang, A laser-processed micro/nanostructures surface and its photothermal de-icing and self-cleaning performance, *Journal of Colloid and Interface Science* (2023).
- [9] Y. Tan, B. Hu, J. Song, Z. Chu, W. Wu, Bioinspired multiscale wrinkling patterns on curved substrates: An overview, *Nano-Micro Letters* 12 (2020) 1-42.
- [10] V. Fernandez, C. Llinares-Benadero, V. Borrell, Cerebral cortex expansion and folding: what have we learned?, *The EMBO journal* 35(10) (2016) 1021-1044.
- [11] A.E. Shyer, T. Tallinen, N.L. Nerurkar, Z. Wei, E.S. Gil, D.L. Kaplan, C.J. Tabin, L. Mahadevan, Villification: how the gut gets its villi, *Science* 342(6155) (2013) 212-218.
- [12] M.B. Hallett, C.J. von Ruhland, S. Dewitt, Chemotaxis and the cell surface-area problem, *Nature reviews Molecular cell biology* 9(8) (2008) 662-662.
- [13] L. Wang, C.E. Castro, M.C. Boyce, Growth strain-induced wrinkled membrane morphology of white blood cells, *Soft Matter* 7(24) (2011) 11319-11324.

- [14] X. Gao, J. Li, T. Li, Z. Su, X. Ma, J. Yin, X. Jiang, Photo-polymerization induced hierarchical pattern via self-wrinkling, *Advanced Functional Materials* 31(49) (2021) 2106754.
- [15] W. Xu, S. Chen, M. Yao, X. Jiang, Q. Lu, A near-infrared-triggered dynamic wrinkling biointerface for noninvasive harvesting of practical cell sheets, *ACS Applied Materials & Interfaces* 13(28) (2021) 32790-32798.
- [16] W. Guo, C.M. Reese, L. Xiong, P.K. Logan, B.J. Thompson, C.M. Stafford, A.V. Ievlev, B.S. Lokitz, O.S. Ovchinnikova, D.L. Patton, Buckling instabilities in polymer brush surfaces via postpolymerization modification, *Macromolecules* 50(21) (2017) 8670-8677.
- [17] X. Fan, C. Deng, H. Gao, B. Jiao, Y. Liu, F. Chen, L. Deng, W. Xiong, 3D printing of nanowrinkled architectures via laser direct assembly, *Science Advances* 8(31) (2022) eabn9942.
- [18] J. Chang, C. Meng, B. Shi, W. Wei, R. Li, J. Meng, H. Wen, X. Wang, J. Song, Z. Hu, Flexible, breathable, and reinforced ultra-thin Cu/PLLA porous-fibrous membranes for thermal management and electromagnetic interference shielding, *Journal of Materials Science & Technology* (2023).
- [19] B. Tang, W.L. Li, Y. Chang, B. Yuan, Y. Wu, M.T. Zhang, J.F. Xu, J. Li, X. Zhang, A Supramolecular Radical Dimer: High-Efficiency NIR-II Photothermal Conversion and Therapy, *Angewandte Chemie International Edition* 58(43) (2019) 15526-15531.
- [20] Z. Zeng, F. Jiang, Y. Yue, D. Han, L. Lin, S. Zhao, Y.B. Zhao, Z. Pan, C. Li, G. Nystrom, Flexible and ultrathin waterproof cellular membranes based on high-conjunction metal-wrapped polymer nanofibers for electromagnetic interference shielding, *Advanced Materials* 32(19) (2020) 1908496.
- [21] C. Keiser, C. Becker, R.M. Rossi, Moisture transport and absorption in multilayer protective clothing fabrics, *Textile Research Journal* 78(7) (2008) 604-613.
- [22] J. Chang, L. Shi, M. Zhang, R. Li, Y. Shi, X. Yu, K. Pang, L. Qu, P. Wang, J. Yuan, Tailor-Made White Photothermal Fabrics: A Bridge between Pragmatism and Aesthetic, *Advanced Materials* (2023) 2209215.
- [23] Z. Lu, B. Zhang, H. Gong, J. Li, Fabrication of hierarchical porous poly (L-lactide)(PLLA) fibrous membrane by electrospinning, *Polymer* 226 (2021) 123797.
- [24] Y. Yu, L. Chen, D. Weng, Y. Hou, Z. Pang, Y. Zeng, J. Wang, Solvent volatilization-induced cross-linking of PDMS coatings for large-scale deicing applications, *ACS Applied Polymer Materials* 5(1) (2022) 57-66.
- [25] H. Jia, J. Guo, J. Zhu, Comparison of the photo-thermal energy conversion behavior of polar bear hair and wool of sheep, *Journal of Bionic Engineering* 14(4) (2017) 616-621.
- [26] W.-H. Han, Q.-Y. Wang, Y.-Y. Kang, X. Zhou, C.-C. Hao, Electrospun polymer nanocomposites for thermal management: a review, *Nanoscale* 15(5) (2023) 2003-2017.
- [27] M. Chung, W.H. Skinner, C. Robert, C.J. Campbell, R.M. Rossi, V. Koutsos, N. Radacsi, Fabrication of a wearable flexible sweat pH sensor based on SERS-active Au/TPU electrospun nanofibers, *ACS applied materials & interfaces* 13(43) (2021) 51504-51518.
- [28] Y. Ahn, D.-H. Hu, J.H. Hong, S.H. Lee, H.J. Kim, H. Kim, Effect of co-solvent on the spinnability and properties of electrospun cellulose nanofiber, *Carbohydrate polymers* 89(2) (2012) 340-345.
- [29] C. Shi, D. Yuan, L. Ma, Y. Li, Y. Lu, L. Gao, X. San, S. Wang, G. Fu, Outdoor sunlight-driven scalable water-gas shift reaction through novel photothermal device-supported $\text{CuO}_x/\text{ZnO}/\text{Al}_2\text{O}_3$ nanosheets with a hydrogen generation rate of 192 mmol g⁻¹ h⁻¹, *Journal of Materials Chemistry A* 8(37) (2020) 19467-19472.

Hosted file

000.graphical abstract.pptx available at <https://authorea.com/users/754736/articles/724582-reinforced-nanowrinkle-electrospun-photothermal-membranes-via-solvent-induced-recrystallization>